# Scanning laser acoustic microscopy using derivative quadrature detection

M. Cywiak and C. Solano
*Centro de Investigaciones en Optica, A.C.*
*Apartado postal 1-948, 37000 León, Gto, Mexico*

G. Wade
*Department of Electrical and Computer Engineering, University of California*
*93106 Santa Barbara, California*
*e-mail: csolano@foton.cio.mx*

Recibido el 10 de julio de 1998; aceptado el 8 de diciembre de 1998

Derivative quadrature detection is proposed for replacing the knife-edge detector currently in use in scanning laser acoustic microscopy. This new system employs an optical $\pi$-step, a reference beam, an electronic quadrature detector and two RAMs for demodulating the laser beam which has been modulated by the acoustically-obtained image information. The $\pi$-step senses the derivative of the object function, the quadrature detector determines its amplitude and sign, and the RAMs combine the results thus obtained for reconstructing the acoustic image. This detector is inherently capable of better resolution than the conventional knife-edge system. A second advantage over the knife-edge is that oblique insonification is not required and a Doppler shift in the detected frequency of the transmitted zero-order acoustic beam is thus avoided.

*Keywords:* Acoustic microscopy; Schliering technique; Fourier optics

Se propone un detector derivativo de cuadratura para reemplazar el detector de navaja que se utiliza convencionalmente en los microscopios acústicos de barrido láser, Este nuevo sistema emplea un escalón de fase $\pi$, un haz de referencia, un detector electrónico de cuadratura y dos memorias de acceso aleatorio para demodular el haz del láser el cual ha sido modulado por la información obtenida acústicamente. El escalón de fase $\pi$ detecta la derivada de la función objeto, el detector de cuadratura determina su amplitud y signo. Las memorias de acceso aleatorio combinan estos resultados para reconstruir la imagen acústica. Este detector presenta mejor resolución que el sistema convencional que utiliza el borde de navaja. Una segunda ventaja sobre el detector de borde de navaja es que no requiere dirigir la onda sonora de excitación de manera oblicua. Esta característica elimina el corrimiento por efecto Doppler en la frecuencia de la onda detectada y permite a su vez incrementar la resolución del sistema y simplificar la electrónica asociada.

*Descriptores:* Microscopía acústica; técnicas Schliering; óptica de Fourier

PACS: 43.60.+d; 42.30.Kq; 42.79.Mt

## 1. Introduction

In acoustic microscopy high-frequency ultrasound is used to observe the internal structure of thin objects. A technology currently in substantial commercial use is called scanning laser acoustic microscopy (SLAM).

SLAM has become a reliable option for obtaining high-quality micrographs in real time with good resolution and contrast. The conventiona thechnique for image data read-out in SLAM is to deflection-modulate a laser beam by scanning it over a solid surface containing the acoustic field scattered from the object and then to demodulate the beam by means of a knife-edge detector (KED). The probing beam is reflected from the surface of a mirrored coverslip onto which the acoustic waves, scattered from the object, impinge (see Fig. 1). The image information is encoded as deflection modulation on the reflected light and is detected by the KED. As shown, the system consists basically of a knife-edge placed in the focal field of a lens with a photodiode positioned behind the knife-edge.

This paper gives a brief description of the operation of the KED in SLAM in which the detected output is proportional to the amplitude of the acoustic surface waves induced on the mirrored coverslip. Then a new detector that we call the derivative quadrature detector (DQD) is described and analyzed. This detector is different from the other detectors so far proposed by its employment of four key components: an optical $\pi$-step, a reference beam, an electronic quadrature detector and two RAMs. The $\pi$-step makes possible the sensing of the derivative of the object function. The reference beam mixes coherently with the modulated probing beam in order to demodulate the acoustical image signal, namely the above derivative. The quadrature detector determines the amplitude and sign of this derivative. The RAMs combine the data thus obtained for reconstructing the acoustic image. We show that the DQD gives better contrast and resolution than other detectors, especially in the vicinity of edges and borders.

The need for more sensitive methods of acoustic data acquisition and image reconstruction of microscopic objects with high resolution has grown. In the literature, a number of

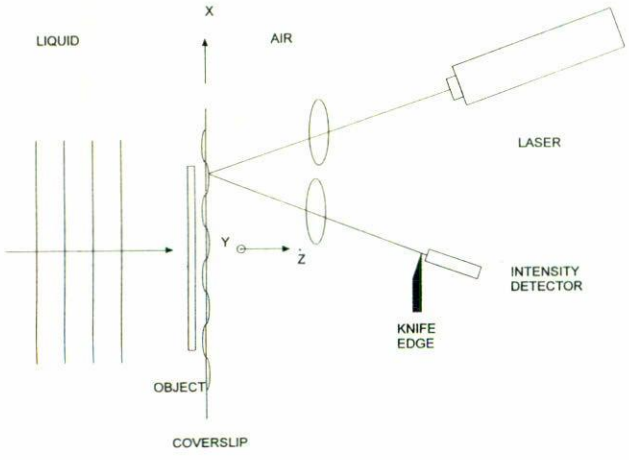


FIGURE 1. Basic set up for the knife edge detector method.

systems for detecting scanned laser acoustic images are described [1–4]. Since SLAM is widely used in many applications [5, 6] novel techniques for data acquisition continue to be studied and proposed [7, 8].

## 2. Slam using knife-edge detection

As stated above, a conventional SLAM employs a KED for the deflection demodulation of the laser beam containing the acoustic image data as illustrated in Fig. 1. To describe the operation of the system, let us consider in some detail how it detects image information.

When an arbitrary microscopic object is insonified by the acoustic beam and is transmitted through it, a dynamic ripple is produced on the mirror-like surface of the coverslip beyond the object. The sinusoidal components of the object function will give rise to terms in the coverslip surface deformation like the following [4]:

$$z(x, y, t) = \mathrm{Re}\left\{h(x, y)\exp(-j\omega, t)\right\}, \qquad (1)$$

where Re indicates "the real part of" and $\omega$ is the temporal frequency of the acoustic beam.

A scanning laser beam is then used to read out the image information concerning the object—that is, to determine the value of expression (1) for each object-function component—by probing the ripple. As it moves, the ripple causes the laser beam to be deflected through an angle proportional to the slope of the surface deformation, specifically the slope indicated in expression (1). Thus the image information is encoded as deflection modulation on the reflected beam and is detected by the KED.

In its most sensitive operation, the deflected beam moves perpendicularly with respect to the knife edge causing the light collected by the photodiode behind the knife edge to be intensity modulated. The diode current is substantially proportional to the laser-beam deflection and therefore to the slope of the surface ripple. This slope, in turn, is proportional to the strength of the sound transmitted through the object.

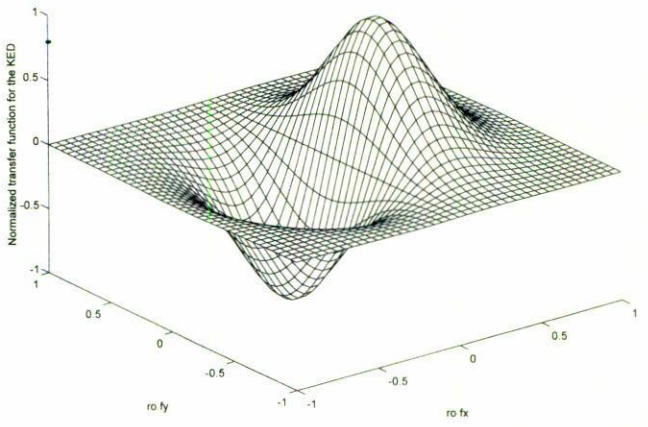


FIGURE 2. Normalized transfer function for the knife edge detector method.

As SLAM operates, the laser beam is caused to scan the surface containing the dynamic ripple. The spatial information modulates the beam and is converted to a corresponding temporal signal by means of the scanning and the knife-edge processing.

Based on the above description, it can be shown mathematically that the transfer function $T_f$ for the KED using a laser beam with a Gaussian intensity profile is given by [9]

$$T_f = \delta_0 \exp\left(-\frac{\pi^2 r_0^2 (f_x^2 + f_y^2)}{2\lambda^2 f^2}\right) \mathrm{erf}\left(\frac{\pi r_0^2 f_x}{\sqrt{2}\lambda f}\right), \qquad (2)$$

where $(f_x, f_y)$ are the spatial frequencies for sinusoidal variations in the transmittance function of the object along the axes $(x, y)$ and $r_0$ is the effective beam radius. The knife edge is assumed to be oriented parallel to the $x$ direction and

$$\mathrm{erf}(x) = \frac{2}{\pi}\int_0^{\infty} \exp(-t^2)\, dt. \qquad (3)$$

A plot with 3-dimensional perspective showing normalized $T_f$ as a function of $r_0 f_x$ and $r_0 f_y$ is shown in Fig. 2.

From Fig. 2 we see that the response vanishes for zero frequency. To avoid operating in this region, the acoustic insonifying waves are directed to fall oblique onto the object. As the laser beam moves to scan out the raster pattern necessary to produce the image, a Doppler shift in the frequency of the detected signal is produced.

In order to stay away from the null response as much as possible, usually only the upper side band is used in the detection process. In spite of the above measures (oblique incidence and single-side band detection) which are employed to widen the useful spatial spectrum, the resolution is still not good. The useful spectrum for effective image reconstruction has to be limited to the positive part of the transfer function and must avoid the null at $f_x = 0$. This results in a correspondingly limited resolution in the reconstructed images.

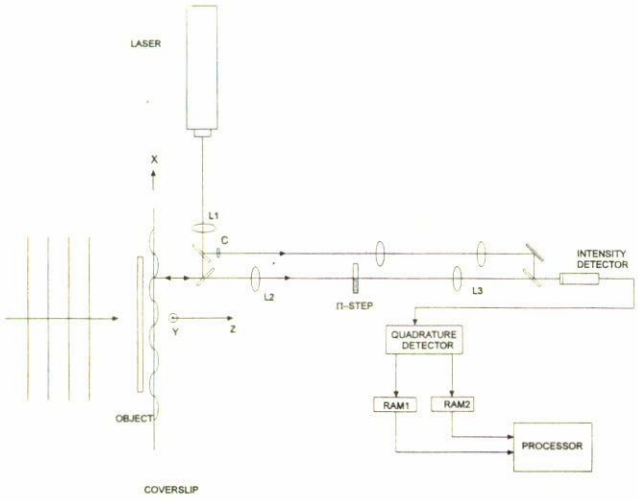


FIGURE 3. The DQD detector system. In the mathematical treatment it has been assumed that all the lenses have the same focal length. C is an optical path length compensator.

## 3. Slam using derivative quadrature detection

We propose a new detection system using a $\pi$-step [10], a reference beam, an electronic quadrature detector and two RAMs as shown in Fig. 3. We analyze the response of the detector considering an object represented in its general form. For simplicity, it will be supposed that all the lenses have the same focal length. If an experimental set up requires different focal lengths the final result will be modified only by a scale factor.

It has been shown that the use of a $\pi$-step, instead of a knife-edge, can improve the accuracy of the image reconstruction in the case of an optical phase object [10]. We will show that for acoustical objects in SLAM a similar improvement can be obtained.

The $\pi$-step is mathematically represented by the sign function defined as

$$\operatorname{sgn}(x) = \begin{cases} +1 & x > 0, \\ -1 & x < 0. \end{cases} \tag{4}$$

Let us suppose the coverslip surface deformation has the general form expressed in Eq. (1). The coverslip is probed by a laser beam with incident power $P$ and a Gaussian intensity profile centered at the point $(x_0, y_0)$

$$\Psi(x,y) = \sqrt{\frac{2P}{\pi r_0^2}} \exp\left[-\frac{(x-x_0)^2 + (y-y_0)^2}{r_0^2}\right], \tag{5}$$

where $\Psi$ is the complex amplitude distribution function of the beam. In order to simplify the equations, the parameters $(x_0, y_0)$ will be suppressed, (that is, assumed to be zero for the time being) and will be appropriately reintroduced in the final result.

The probing beam, after being reflected from the surface of the coverslip is phase- and amplitude-modulated by the dynamic ripple. Thus the reflected complex amplitude distribution function is given by

$$\Psi_r = \sqrt{\frac{P}{\pi r_0^2}} \exp\left(-\frac{x^2+y^2}{r_0^2}\right)[1 + jkh(x,y)\exp(-j\omega,t) + jkh^*(x,y)\exp(j\omega,t)], \tag{6}$$

where $k = 2\pi/\lambda$, the light wavelength. In Eq. (6) only terms of the first order in $\lambda$ have been retained due to the fact that the value of this product is very small compared with unity.

Lens L2 performs the Fourier transform of $\Psi_r$, and after passing the $\pi$-step plane, we have

$$\Psi_r = \sqrt{\frac{P}{\pi r_0^2}}\left(\frac{\pi r_0^2}{j\lambda f}\right)\left\{\exp\left(-\pi r_0^2 \frac{\xi+\eta^2}{(\lambda f)^2}\right) \otimes \left[\delta\left(\frac{\xi}{\lambda f}, \frac{\eta}{\lambda f}\right) + jkH\left(\frac{\xi}{\lambda f}, \frac{\eta}{\lambda f}\right)\exp(-j\omega_s t) + jkH^*\left(-\frac{\xi}{\lambda f}, -\frac{\eta}{\lambda f}\right)\exp(j\omega_s, t)\right]\right\}\operatorname{sgn}(\xi) \tag{7}$$

where $(\xi, \eta)$ are the coordinate axes at the plane of the $\pi$-step, $H(\xi,\eta) = F\{h(x,y)\}$ the Fourier transform of the object function $h(x,y)$ and $\otimes$ denotes the convolution operation.

Lens L3 performs the Fourier transform of $\Psi_P$, giving

$$\Psi_f = -\sqrt{\frac{P}{\pi r_0^2}}\frac{1}{\lambda^2 f^2}\exp\left(-\frac{u^2+v^2}{r_0^2}\right)[1 + jk\lambda^2 h(-u,-v)\exp(-j\omega_s,t) + jk\lambda^2 f^2 h^*(-u,v)\exp(j\omega_s,t)] \otimes \left(\frac{\lambda f}{j\pi u}\right), \tag{8}$$

where $(u, v)$ represent the coordinate axes at the intensity detector plane (Fig. 3).

Writing the convolution as an integral, we have

$$\Psi_f = -\sqrt{\frac{P}{\pi r_0^2}}\left(\frac{1}{\lambda f}\right)\exp\left(-\frac{v^2}{r_0^2}\right)\left[\frac{1}{j\pi}\int_{-\infty}^{\infty}\frac{\exp\left(-\frac{s^2}{r_0^2}\right)}{u-s}\,ds\right.$$

$$\left.+k\lambda^2 f^2\exp(-j\omega_s,t)\frac{1}{\pi}\int_{-\infty}^{\infty}\frac{\exp\left(-\frac{s^2}{r_0^2}\right)h(-s,-v)}{u-s}\,ds + k\lambda^2 f^2\exp(j\omega_s,t)\frac{1}{\pi}\int_{-\infty}^{\infty}\frac{\exp\left(-\frac{s^2}{r_0^2}\right)h^*(-s,-v)}{u-s}\,ds\right] \quad (9)$$

$s$ being an auxiliary dummy variable. Thus

$$\Psi_f = -\sqrt{\frac{P}{\pi r_0^2}}\frac{1}{\lambda f}\exp\left(-\frac{v^2}{r_0^2}\right)\left\{\frac{1}{j}H_i\left[\exp\left(-\frac{s^2}{r_0^2}\right)\right] + k\lambda^2 f^2\exp(-j\omega_s,t)H_i\left[\exp\left(-\frac{s^2}{r_0^2}\right)h(-s,-v)\right]\right.$$

$$\left.+k\lambda^2 f^2\exp(j\omega_s,t)H_i\left[\exp\left(-\frac{s^2}{r_0^2}\right)h^*(-s-v)\right]\right\} \quad (10)$$

where $H_i\{X(s)\}$ denotes the Hilbert transform of $X(s)$ and is defined by [11, 12]

$$H_i\{X(s)\} = R(u) = \frac{1}{\pi}\int_{-\infty}^{\infty}\frac{X(s)}{u-s}\,ds, \quad (11)$$

with the inversion formula

$$X(u) = \frac{1}{\pi}\int_{-\infty}^{\infty}\frac{R(s)}{u-s}\,ds. \quad (12)$$

Using D'Velis approximation [13] $\frac{1}{s^2} \approx \delta(s)$ for small values of $s$, we can write Eq. (10) as

$$\Psi_f = -\sqrt{\frac{P}{\pi r_0^2}}\frac{1}{\lambda f}\exp\left(-\frac{v^2}{r_0^2}\right)\left\{\frac{\pi}{j}\frac{d}{du}\left[\exp\left(-\frac{u^2}{r_0^2}\right)\right] + k\lambda^2 f^2\pi\frac{d}{du}\left(Re\left[h(-u,-v)\exp\left(-\frac{u^2}{r_0^2}\right)\exp(j\omega_s,t)\right]\right)\right\}. \quad (13)$$

Only values near the optical axis are considered, *i.e.*, $\mid u \mid \ll 1$, and the last relation can be written as:

$$\Psi_f = -\sqrt{\frac{P}{\pi r_0^2}}2\pi^2 f\exp\left(-\frac{u^2+v^2}{r_0^2}\right)\frac{d}{du}\left[\mathrm{Re}\left\{h(-u,-v)\exp(j\omega_s,t)\right\}\right]. \quad (14)$$

As shown in Fig. 3, a reference beam is coherently added to the amplitude function $\Psi_f$ (A similar result has been described before in the case of a reference beam advanced or retarded by 90° [14]. In the system of the present paper this change of 90° is not necessary because the $\pi$-step advances the signal by the same 90°). The reference beam needs to be Fourier transformed twice so that it has the same functional form as the signal beam.

Thus the reference beam at the plane of the detector will be given by

$$\Psi_R = -\sqrt{\frac{P}{\pi r_0^2}}\exp\left(-\frac{u^2+v^2}{r_0^2}\right), \quad (15)$$

The total amplitude, $\Psi_T$, at the plane of the detector of Fig. 3, is

$$\Psi_T = \Psi_f + \Psi_R.$$

Therefore, the power detected by the intensity detector is

$$P_I = \frac{4P\pi f}{r_0^2}\int_{-\infty}^{\infty}\int_{-\infty}^{\infty}\exp\left[-2\frac{(u^2-u_0^2)^2+(v^2-v_0^2)^2}{r_0^2}\right]$$

$$\times\frac{d}{du}\left[\mathrm{Re}\left\{h(-u)\exp(j\omega_s,t)\right\}\right]du\,dv. \quad (16)$$

where the values $(x_0, y_0)$ have been reintroduced. This equation has the mathematical form of a convolution of the derivative of the object function with the response of the system. Let us define $\mathcal{F}_s(u,v)$ as follows:

$$\mathcal{F}_s(u,v) = \frac{4Pf}{r_0^2}\exp\left(-2\frac{u^2+v^2}{r_0^2}\right). \quad (17)$$

Equation (17) shows that $\mathcal{F}_s(u,v)$ is Gaussian and isotropic with its maximum at the origin. This fact indicates that for best operation we should insonify at normal incidence.

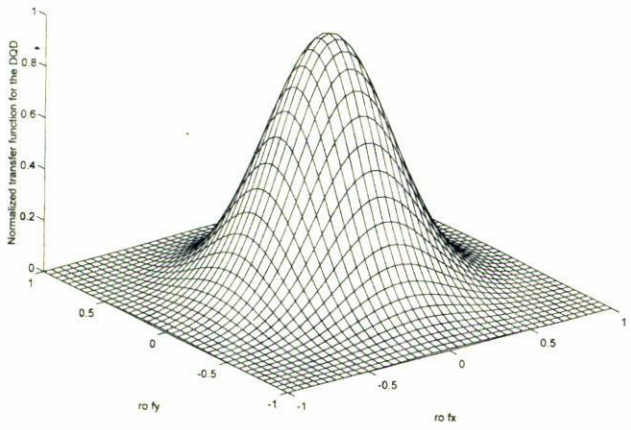


FIGURE 4. Normalized transfer function of the DQD detector system.

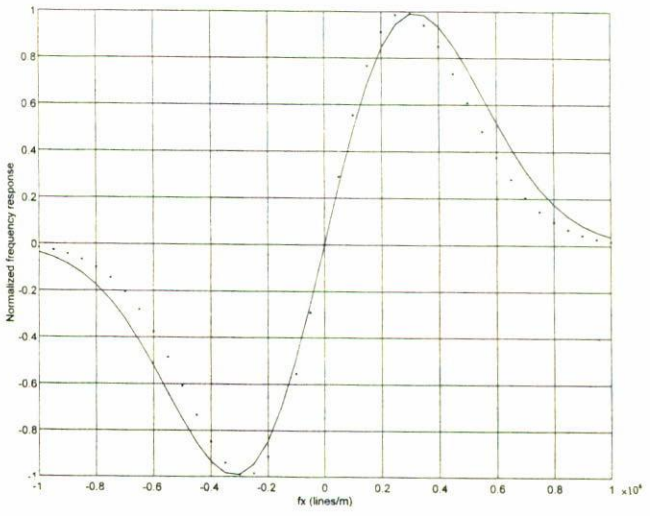


FIGURE 5. Comparison of the KED *vs.* DQD frequency response for $r_0 = 1\,\mu$. (The continuous trace corresponds to the DQD) Note that although in the plot the bandwidth increase for the DQD appears small, the actual improvement is $\approx 10^5$ lines/m.

In order to be able to compare the spatial frequency response of the system with that of the KED, we must now obtain the transfer function for the DQD. As was stated before, it is enough to consider one spectral component of the object. By Fourier transforming Eq. (16 ) we obtain for the transfer function of the system

$$T_{\mathrm{DQD}}(f_x, f_y) = j2P\pi f_x \exp\left[-\frac{\pi^2 r_0^2}{2}(f_x^2 + f_y^2)\right], \quad (18)$$

where $f_x, f_y$ are the spatial frequencies in both coordinate axes.

The normalized transfer function $T_{\mathrm{DQD}}(f_x, f_y)$ is shown with three dimensional perspective in Fig. 4. In Fig. 5 we show one-dimensional normalized views where $f_y = 0$ for the two detectors for $r_0 = 1\ \mu$m. From this figure it can be seen that the spatial frequency response is broader for the DQD by approximately 105 lines/m than for the KED.

To obtain an insight into the meaning of Eq. (16), we can expand de complex function $h'(-u)$ as a product of its magnitude and its phase $\alpha$ as follows

$$h'(-u) = \mid h'(-u) \mid \exp(-j\alpha(-u), \quad (19)$$

where $h'(-u) = (d/du)h(-u)$. And then express Eq. (16) as

$$P_I = \frac{4Pf}{r_0^2}\int_{-\infty}^{\infty}\int_{-\infty}^{\infty}\exp\left[-2\frac{(u-u_0)^2 + (v-v_0)^2}{r_0^2}\right] \times \mid h'(-u) \mid \cos(\omega_s, t + \alpha)\, du\, dv. \quad (20)$$

## 4. Functional description of the DQD

According to Eq. (20), the ac signal received by the intensity detector of Fig. 3, varies with the amplitude and the phase of the derivative of the object function. In order to determine the amplitude and the phase separately, we use a quadrature detector [15]. As the laser beam scans over the coverslip, at each object point the quadrature detector will determine the two quantities. Both are then stored in the two RAMs indicated in Fig. 3: the value $\mid h'(-u) \mid$ being stored in the first RAM and the value of $\alpha$, in the second. These two quantities are then manipulated to form the product $\mid h'(-u) \mid \cos(\alpha)$, that is, the real part of the derivative of the object function. If $\alpha$ is too large an unwrapping method may be needed [16].

We obtain the image by reconstructing a reversed object function, $h(-u)$. The following example will illustrate how this is done.

Suppose the object is the rectangle shown in Fig. 6a. Its mathematical derivative then consists of two delta functions. As the optical system of the DQD is sensitive to the derivative it will approximately detect these two functions, as illustrated ideally in Fig. 6b. The corresponding derivative of $h(-u)$is stored in RAM 1 as shown in Fig. 6c. The phase of this derivative is stored in RAM 2 as shown in Fig. 6d. Finally, in Fig. 6e we shown the reconstructed function $h(-u)$ as obtained by the computer. This reconstruction involves integrating the data stored in RAM 1, making use of the correct sign from the data stored in RAM 2.

## 5. Discussion and conclusions

One disadvantage of the DQD system is that processing time is needed to integrate the data in each scanning line. Thus the system cannot operate in real time. Nevertheless, as the speed of computer processors is now very high, this processing time may be as short as a few milliseconds.

With KED, the operation is in real time but serious problems are encountered for objects containing high spatial frequencies due to insufficient resolution of edges and borders.

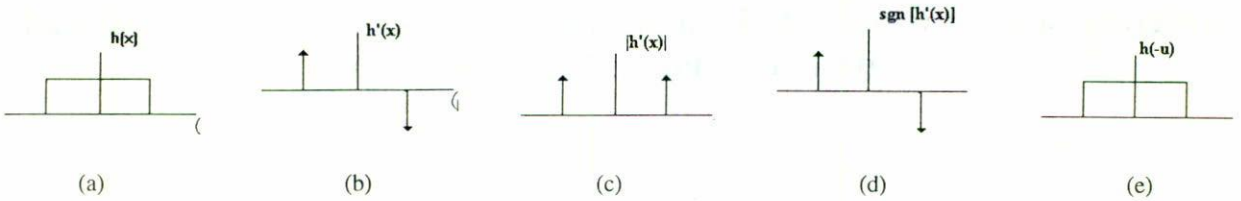


FIGURE 6. Simple example of imaging with the DQD. a) Original object; b) The derivative of a) obtained by the optical system; c)The intensity recorded by the detector; d)The phase stored at RAM 2; e) Recovered image.

The proposed DQD detection system provides better response at higher frequencies, making it useful to detect edges and borders because its response is sensitive to the derivative of the signal. In addition, the DQD may be used with normal insonification which does not give rise to a Doppler shift in the insonifying frequency.

The DQD gives a transfer function for the derivative of the object function that is symmetrical with a maximum response at the origin. This avoids the necessity of oblique insonification that is required with the KED, thus eliminating the resultant Doppler shift in the detected signal due to scanning. The fact that the transfer function is well behaved, has the additional advantage that it greatly simplifies the associated electronics.

Among the most important results is that the DQD responds to the complex derivative of the object function, a response not possible with the conventional SLAM. Furthermore, the frequency response of the DQD is broader than the KED therefore images of better resolution and contrast are inherently obtainable with the DQD.

## Acknowledgment

This work was supported in part by a CONACYT scholarship to M Cywiak, Conacyt proyect 4196P A and a 1996 UCMEXUS grant for Scanning-Laser Acoustic Microscopy to G. Wade.

1. A. Korpel and P. Desmares, *J. Acoust. Soc. Am.* **45** (1969) 881.
2. L. Whitman and A. Korpel, *Appl. Opt.* **8** (1969) 1567.
3. L. Kessler, *Acoustic Imaging*, (Plenum, New York, 1976) p. 299.
4. R. Mueller and R. Rylander, *J. Opt. Soc. Am.* **69** (1979) 407.
5. R.M. Kent, *Final Report*, Dayton Univ, Oh., March (1993).
6. Y. Kim, W.D. Hunt, Y. Liu and C. Jen, *J. Appl. Phys.* **76** (1994) 1455.
7. S. Samson, A. Korpel, and H.S. Snyder, *Int. J. Immaging Syst. Technol* **7** (1996) 48.
8. A. Meyyappan *et al.*, *Int. J. Img. Syst. and Tech.* **7** (1996) 131.
9. M. Cywiak, Tesis Doctoral, CIO, León, Gto., México, 1998.
10. S. Lowenthal and Y. Belvaux, *Appl. Phys. Lett.* **11** (1967) 49.
11. M. Born and E. Wolf, *Principles of Optics*, (Pergamon Press, Oxford, England, 1975) p. 425.
12. A. Papoulis, *Systems and Transforms with Applications to Optics*, McGraw-Hill, New York, 1977) p. 251.
13. J. DeVelis and G. Reynolds, *Theory and Applications of Holography*, (Addison-Wesley, Reading, MA, 1967) Chap. 8.
14. M. Cywiak, C. Solano, G. Wade and S. Isakson, *J. Acoust. Soc. Am.* **103** (5) (1998).
15. H. Lee and C. Ricci, *Appl. Phys. Lett.* **49** (1986) 1336.
16. M. Servin and F.J. Cuevas, *J. Mod. Opt.* **42** (1995) 1853.